CCFE
CULHAM CENTRE FOR FUSION ENERGY

UK Atomic Energy Authority

UKAEA-CCFE-PR(20)02

Ryan Sperry, David T Fullwood, Allan Harte, Joao Quinta da Fonseca, Eric R Homer, Robert H Wagoner

Slip band characteristics in the presence of grain boundaries in nickel-based superalloy

Slip band characteristics in the presence of grain boundaries in nickel-based superalloy

Ryan Sperry, David T Fullwood, Allan Harte, Joao Quinta da Fonseca, Eric R Homer, Robert H Wagoner

This is a preprint of a paper submitted for publication in Acta Materialia

Slip band characteristics in the presence of grain boundaries in nickel-based superalloy

Ryan Sperry[1], David T Fullwood[1], Allan Harte[2,3], Joao Quinta da Fonseca[2],
Eric R Homer[1], Robert H Wagoner[4]
[1] Brigham Young University, Provo, Utah, USA
[2] The University of Manchester, UK
[3] UKAEA, Culham Science Centre, Abingdon, Oxon, OX14 3EB,
[4] The Ohio State University, Columbus, Ohio, USA

Abstract

Shear strain profiles along slip bands in a modified Rolls-Royce nickel superalloy (RR1000) were analyzed for tensile sample deformed by 2%. The strain increased with distance away from a grain boundary (GB), with maximum shear strain towards the center of the grain, indicating that dislocation nucleation generally occurred in the grain interior. The strain gradients in the neighborhood of the GBs were quantified and showed rotation about the active slip system line direction. The dislocation spacing and pileup stresses were inferred. The dislocation spacing closely follows an Eshelby analytical solution for a single ended pileup of dislocations under an applied stress.

The distribution of pileup stress values for GBs of a given misorientation angle between both grains follows a log-normal distribution, with no correlation between the pileup stress and the GB misorientation angle. Furthermore, there is no observed correlation between various transmissivity factors and slip band pileup stress. Hence it appears that the obstacle strength of any of the observed GBs is adequate to cause the dislocation pileups present in the slip bands.

Slip band transmission is influenced by transmissivity factors with particular interest in the Luster and Morris m'-factor. Transmission occurs at higher m' values, except at twin boundaries which show transmission peaking at m' values of 0.78. Observation of strain profiles of transmitted bands show dislocation nucleation in one grain, both grains, and at the grain boundary.

Introduction

Despite the known importance of dislocation / grain boundary (GB) interactions, most mesoscale models do not account for these interactions at the slip system level. A large factor in this technological gap is the lack of detailed observations of dislocation / GB interactions across the wide range of GB types. While the observation of single dislocation behavior in the presence of GBs is difficult to observe at for a statistically significant number of cases, slip-band interactions can be observed much more readily using various techniques.

This paper employs high-resolution digital image correlation (HRDIC), combined with electron backscatter diffraction (EBSD) to study slip band interactions with GBs for many bands, across a wide range of GBs. The nature of the underlying slip activity, the associated geometrically necessary dislocation (GND) structure and resultant stress concentrations, and the transmission behavior across GBs is investigated.

Slip bands are the dominant mechanism for plastic deformation in a range of polycrystalline materials. For face-centered cubic (FCC) nickel-based superalloys, there are generally one or more favorably oriented slip systems for accommodation of strain within each grain, often resulting in a single dominant system of parallel slip bands across the grain. However, the behavior of the bands as they approach grain boundaries (GBs) can be more varied, with some bands crossing, and others fizzling out or breaking up as they approach the obstacle.

In the classical view of the slip band / GB interaction, proposed by Hall and Petch [1,2], dislocations that form in the grain interior glide until they encounter a GB that prevents further motion; dislocations following behind a pinned dislocation are repelled by the elastic dislocation-dislocation forces, and a pileup occurs (see Li and Chou for a discussion of this scenario, and alternative hypotheses [3]). Of particular importance in this view is the GB obstacle strength – the stress required to push the dislocation into or through the boundary. Hence the fundamental question arises as to whether the observed pileup and / or the transmission behavior at GBs correlates with GB obstacle strength.

Measured or calculated values of obstacle strength are not available for most GBs, in any material; some inferred values exist for a limited number of observations (e.g. [4]), and various analyses of certain GB subsets have been attempted with molecular dynamics (e.g. [5]). Nevertheless, there is a generally accepted notion that the obstacle strength will correlate with geometrical transmissivity factors [6]that quantify the misalignment of incoming and outgoing slip systems. Thus, the current paper investigates the existence of correlations between these transmissivity factors and both the observed pileup stresses and observed transmission behavior.

Slip band identification

A polycrystalline nickel superalloy specimen was investigated: RR1000 with γ’ precipitate. The γ/ γ’ alloy was subjected to heat treatment in order to arrive at unimodal size distributions of γ’ precipitates with diameters of ~70 nm. Details of the heat treatment are given in [7]. The average grain size (equivalent circle diameter) for the alloy was approximately 20 μm.

A tensile specimen was machined and polished for pre-deformation EBSD orientation mapping using standard mechanical polishing processes [7]. Then, a gold speckle pattern was applied to the sample surface for the image correlation process, following the procedure detailed in [8].

Images of the speckle pattern were obtained before and after uniaxial tensile deformation, in the unloaded state, and the resulting displacement field was calculated using daVis [9].

Backscattered electron images of the gold speckle pattern were obtained before and after the deformation step using a FEI Magellan HR 400L FE-SEM. To maximise the spatial resolution, the microscope was operated at a voltage of 5 kV with a +2 kV stage bias and a probe current of 0.8 nA. A working distance of 4 mm was chosen to maximise the signal-to-noise ratio. A mosaic of 40 columns x 20 rows was used to collect 800 images with a 20% overlap, corresponding to a field of view of ~ 1 x 0.5 mm. Each image had a resolution of 2048 x 1768 pixels and a pixel size of 14.6 nm.

The dogbone sample was deformed in uniaxial tension using a Zeiss-Kammrath 5 kN tension-compression microtester. The sample was deformed at a rate of 0.3 mm min^{-1} to a global macroscopic uniaxial engineering strain of ~ 0.02.

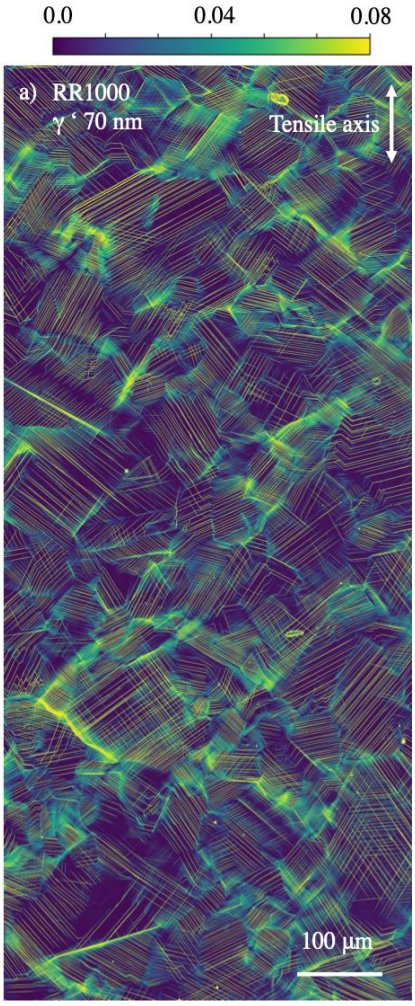

Figure 1. Maximum shear maps from HRDIC analysis of RR1000 with precipitates.

The locally calculated values of displacement, u and v, from DaVis, were used to determine the maximum shear strain, under a 2D plane strain assumption [10]:

$$\frac{\gamma_{max}}{2} = \sqrt{\left(\left(\frac{\partial u}{\partial x} - \frac{\partial v}{\partial y}\right)/2\right)^2 + \left(\left(\frac{\partial u}{\partial y} + \frac{\partial v}{\partial x}\right)/2\right)^2} \quad (1)$$

Note that the level of shear across a slip band was measured relative to the step size of the DIC grid (117nm for the DIC window size of 8x8 pixels) and does not represent the actual shear based upon the distance between neighboring slip planes. This does not affect the calculations of dislocation spacing below, which are based upon the displacements across the slip plane. The resultant strain maps have sharp bands of high shear strain values along the slip bands, as illustrated in Figure 1.

The HRDIC map was spatially registered with the maps of EBSD data by manually selecting a series of triple junctions in both maps and minimizing the least square error between these keypoint positions while applying a linear transformation to the EBSD map. We note that this does not give perfect alignment, with grain boundary positions in the two maps typically being displaced from each other by a few microns. Grains in the DIC map were defined using the EBSD data and were analyzed individually for slip band activity.

The strain map for the grain was passed through a Radon transform, and the peak values indicated the slip band locations. Shear strain vs distance from the GB along the band was extracted from the HRDIC shear strain map. Because of the small error between GB location as defined by the overlaid EBSD map, and the actual GB location in the DIC map, the ends of the slip bands were generally defined by the point of minimum shear value rather than the approximated GB position, significantly mitigating the slight misalignment issue. Spacing between bands were measured by taking perpendicular lines from the center of each identified band, mapping the shear strain along this line, and finding the distance to the first peak, indicating the distance to the neighboring band. This was performed automatically using the findpeaks function in MATLAB, but was also checked manually over a significant number of bands.

Each slip band was automatically identified, and then manually checked by examining the proposed endpoint positions on the shear and EBSD maps, as well as the associated shear profiles along the bands. This was done for each band to confirm the automated program had successfully selected a slip band. We also note that shear bands that are not straight (e.g. that zig-zag across the grain), or that are particularly weak, would not be identified by the Radon transform method. After the automatic identification and manual check process was completed, 660 bands were available for examination.

For each slip band, perpendicular lines were defined, and the relative displacement ratio (RDR), $(u_2 - u_1)/(v_2 - v_1)$, across the band was determined, as described by Chen and Daly [11]; u_1 and u_2 represent displacements of two points on either side of the shear band in the global x-direction, and similarly for the y-direction displacements represented by v_i. For the known crystal orientation (measured by EBSD), potential slip planes whose traces aligned closely with the observed slip band were determined. The measured RDR was then compared with the possible RDRs relating to the identified slip plane(s). Thus, the active slip system associated with the selected band was determined. Once this was known, the component of displacement perpendicular to the sample surface could be determined from the measured x and y displacements (assuming that only a single slip system was active, which generally appears to be true within a slip band). Chen and Daly did validation studies on slip systems identified with high confidence through other methods. Their method proved to match well with predictions from these validation studies.

The Frank-Read source and dislocation loops

The relative displacement across slip bands indicates the number of dislocations that have passed along the slip plane; e.g. for a slip plane that lies in the x-z plane, with an edge dislocation line parallel to the z-axis and with a slip direction along the x-axis, the total relative displacement across the slip band will be nb, where n is the number of dislocations that have passed a given point, and b is the size of the Burgers vector. To create the observed sharp slip

bands shown in the HRDIC scans, there must be consistent successive generation of dislocations on the slip plane. This effect can be attributed to Frank-Read sources [12] which are generally caused by applied stress to pinned dislocation line segments.

In the presence of a barrier to dislocation glide, such as a grain boundary, a dislocation pileup of successive Frank-Read dislocation loops may occur against the locked dislocation that is closest to the barrier. In this case, there is a strain gradient in the direction of the pileup. If all dislocations originated at the center of the grain (consistent with observations detailed below), and if the spacing of the dislocations at a certain value of x is w, then the displacement gradient, $\frac{du}{dx}$, and strain gradient, $\frac{d\varepsilon}{dx}$, at that point (on the side of the slip plane with the dislocation motion) will be given by:

$$\frac{du}{dx} = \frac{b}{w} \;\; ; \;\; \frac{d\varepsilon}{dx} = \frac{-b}{w^2}\frac{dw}{dx} \tag{2}$$

The resultant dislocation spacing and strain gradients can be compared with Eshelby's analytical solutions for the distribution of dislocations in pileups. We consider 1) A double ended pileup between two pinned dislocations, with no externally applied stress, and 2) A single directional pileup against a pinned dislocation, under evenly applied stress [13]. The solution for dislocation positions in the first case is given by the roots of the first derivative of the Legendre functions, and represents a set of more evenly distributed dislocations compared with the second case, where the pileup is more severe near the pinned dislocation; the positions of dislocations for this case are given by the roots of the first derivative of the Laguerre functions.

Figure 2. Illustration of the lattice rotation about the dislocation line direction in a pileup.

A further characterization of GND distributions towards the ends of slip bands was carried out by analyzing the orientation gradient field in the vicinity of the band. In the scenario of a series of edge dislocations aligned along the slip plane, in the slip direction, the crystal lattice should rotate about the dislocation line direction, as shown in Figure 2, by an amount that relates directly to the dislocation density. For n edge dislocations in the step Δx along the slip direction, the lattice curvature is given by [14]:

$$K = \frac{d\theta}{dx} = \frac{d\gamma}{dx} = \rho b \tag{4}$$

where $\rho = 1/(wh)$ for a spacing w between the dislocations in the band, and a spacing h between bands. The measured axis of rotation can then be compared to the line direction of the slip band evaluated using the RDR method.

Furthermore, the direction of the rotation would suggest which portion of the dislocation loop is observed at the surface. Dislocation loops are composed of edge dislocations of opposite signs at either end of the loop (top and bottom of the loop in **Error! Reference source not found.**) with screw dislocations between the edge dislocations [15]. The relative signs of observed edge dislocation pileups will depend on which portion of the loop is observed at the surface. Furthermore, if edge dislocation pileups are observed at both ends of a slip band, the relative signs of the edge dislocations determined from the local rotation gradients. When the rotation direction at each end of the band is calculated using the center of the band as a reference point, rotations of the same direction at each end would suggest edge dislocations of opposite signs at each end. Rotations of the opposite direction would suggest edge dislocations of the same sign in both of the pileups at each end.

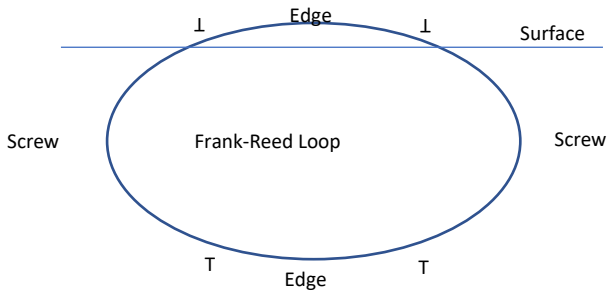

Figure 3. Simple diagram of Frank-Read loop interacting with the sample surface showing edge dislocations of the same sign at the surface. If the loop was rotated 90 degrees, the dislocations observed at the surface would be of opposite sign.

Analysis of Pileups

Of particular interest to the current study is the stress applied to the grain boundary by dislocation pileups within a slip band, and any observed correlations between this stress and the GB character. Eshelby showed that for a pileup caused by an applied stress, τ, the stress on the pinned dislocation would be given by $N\tau$, where N is the number of dislocations in the pileup. For the case of the pileups observed in the nickel superalloy grains, with unknown residual stress after unloading the sample, the pileup stress might be approximated by fitting Eshelby's solutions (such as those mentioned above) to the observed strain gradient and backing out the associated stress. However, a more direct approach involves analysis of the dislocation spacing that is required to produce the observed strain gradient, and then integration of the elastic forces applied by such a dislocation field upon the pinned dislocation. For edge dislocations moving in the same slip plane, the applied stress is summed over a set of integration steps with n_i dislocations in the given step (derived from w in Eq. 2), at a distance x_i from the pinned dislocation [16,17]:

$$\sigma_{xy} = \sum \frac{\mu b n_i}{4\pi(1-\nu)} \frac{l}{x_i\sqrt{x_i+l^2}} \tag{3}$$

where μ is the shear modulus, ν is the Poisson's ratio, and l is the length of the dislocation - taken to be the visible grain diameter in this work. We note that the grain diameter estimate will be a source of variability in the results; but since the stress contribution is higher for small x_i, when the l terms approximately cancel, this should not cause a large error.

Since the total force is most affected by the dislocations closest to the pinned dislocation, the integral of force is sensitive to step sizes used on data close to the pinned dislocation. To maximize computation efficiency and speed, a smaller step size equal to the magnitude of the burgers vector of one dislocation (approximately .104 nm) was used for the first three microns of each shear band. The rest of the band used a step size of .05 microns. It was found that using this step size beyond the first three microns had insignificant effect on the calculated stress when compared to using a step size of the burgers vector for the entire shear band. The data from the DIC maps were interpolated to these refined step sizes, and locally smoothed to reduce numerical noise.

It should be noted that the data was extracted in the unloaded conditions, and hence does not indicate the maximum stress that was applied to the GB by the shear band under load. But it is assumed that the unloaded strain will be proportional in some way to the loaded value.

Transmissivity Factors and Transmission

As previously noted, one objective of the current study is to determine correlations between pileup stress exerted on GBs, and microstructural metrics that might relate to the obstacle stress of the given boundaries. Metrics that have arisen in the literature include the Luster and Morris m'-factor, as given by [18]:

$$m' = \max_{\alpha}\{\hat{n}_{sb} \cdot \hat{n}_{\alpha} * \hat{b}_{sb} \cdot \hat{b}_{\alpha}\} \tag{5}$$

where $\hat{n}_{sb}$ and $\hat{b}_{sb}$ are unit vectors perpendicular to the slip plane and in the direction of slip, respectively for the shear band being examined; and $\hat{n}_{\alpha}$ and $\hat{b}_{\alpha}$ are unit vectors for all slip systems in the neighboring grain.

Other factors such as the Chalmers N-Factor [19], the Lambda parameter from Werner and Prantl [20], and the residual Burgers vector (RBV) [21] were used to measure transmissivity. However, as will be seen below, this study focused on m' and misorientation because they are common metrics in the literature and showed typical results of the other transmissivity factors..

Higher values of metrics m', N and λ indicate better aligned slip systems across the GB, and hence easier transmission. For the RBV metric, a high value indicates that for a dislocation to transmit through the GB, if the net Burgers vector is conserved, a high residual Burgers vector must be retained in the GB, presumably at a high energetic cost, thus correlating with more difficult transmission.

Other microstructural attributes that may correlate with transmissivity include the misorientation of the GB of interest, along with other metrics such as combinations of Schmid or Taylor factors of the neighboring grains.

Transmission

As mentioned previously, one type of interaction that can be readily observed between slip bands and GBs is transmission events. If a slip band is transmitting through a GB, then the HRDIC scans should be able to pick up on the continuous shear through the GB caused by the transmitted dislocations. We note that if a transmission event nucleated below the surface, there may be no reason for the slip bands on either side of the GB to line up at the surface. However, there is some evidence to indicate that transmission events primarily nucleate at the free surface, when such a surface is present. The character of strain and strain gradients in slip bands at grain boundaries, for both visibly transmitting and non-transmitting bands, was catalogued to identify a useful classifier for automatically determining if a band transmitted or not. The bands classified as transmitting bands were then compared with transmissivity factors mentioned above to see if there were any correlations between transmission and these factors.

The shear profiles of transmitted bands were also analyzed to obtain insight on the primary source of dislocations for the bands in both non-transmitting and transmitting cases. Since shear is proportional to the number of dislocations that have passed along a slip plane, local maxima, minima, and gradients of the shear profiles can be useful indicators of the source and evolution of the dislocations in these bands.

Results and Discussion

Using the automated method described above 660 bands were identified in the RR1000 material. Note that modifying the parameters of the Radon transform search method would alter the number of bands that are found in the material. A typical plot showing the distance along a slip band vs maximum calculated shear can be seen in Figure 4. Note that the maximum shear is near the grain center. As shear is proportional to the number of dislocations that have

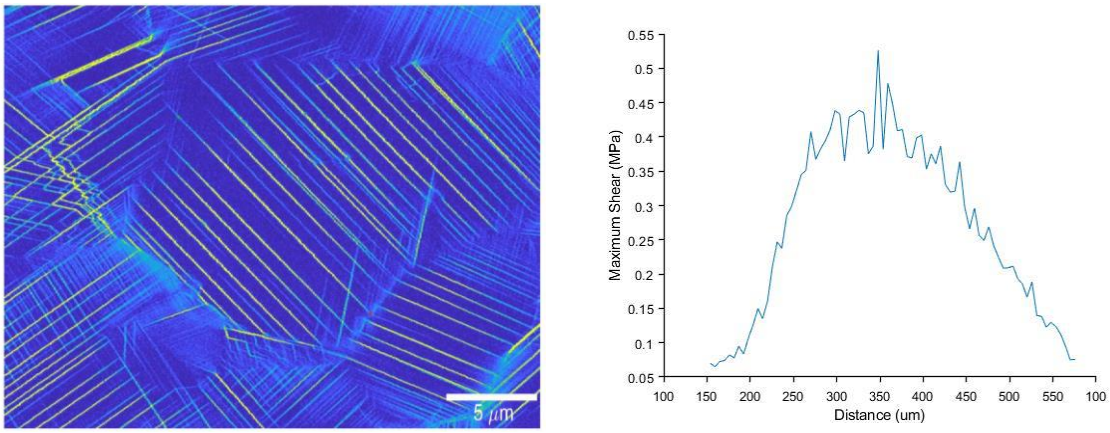

Figure 4. Typical map of maximum shear from HRDIC scanning with visible slip bands (left) and typical shear profile of maximum shear vs. distance along the band starting at one GB and moving toward the other (right).

passed a point, this maximum in the middle of the grain indicates the location of the dominant dislocation source. The majority of shear bands showed similar behavior.

Figure 5**Error! Reference source not found.** presents a boxplot of the normalized shear data along the 660 slip bands in the RR1000 material. The shear profile for each band is normalized to a maximum value of 1, and a width of 20 arbitrary units (a.u). Starting at the GB at one end of a slip band, the median profile of shear increases for the first third of the slip band, levels out for the middle third, and then decreases for the final third of its length, as the opposite GB is approached. As mentioned earlier, this was compared to the solutions proposed by Eshelby for shear strain in dislocation pileups. Since the sample is in the unloaded state, one might assume that the first Eshelby solution (dislocation pileup between two pinned dislocations with no applied stress) would be more relevant; however, the second Eshelby solution actually appears to be a significantly better fit to the data. Hence, it appears that after the sample is unloaded, the dislocations in the slip band do not fully reverse to take the spacing of the ideally unloaded pileup. The resultant dislocation arrangements lead to long-range backstresses.

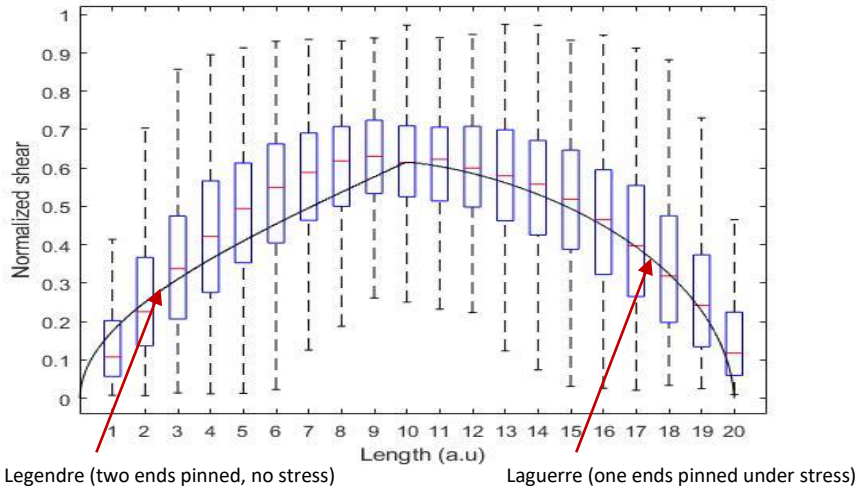

Figure 5. Box plot showing the normalized shape of shear profiles across 660 slip bands in RR1000 fine precipitate material (the middle lines show the median, the box shows 25th-75th percentile values, and the dashed lines show the extent of the other non-outlier values); solutions from two Eshelby pileup scenarios overlaid on the box pot.

As mentioned earlier, the strain gradients caused by these dislocation pileups correlate with orientation gradients in the material. In the RR1000 material, 20 bands were selected by randomly choosing 10 grains and then randomly selecting 2 bands per grain. These bands were used to evaluate these orientation gradients. It was found that 85% (17 of the 20) of the selected bands showed rotation about an axis that matched up with the line direction as identified using the RDR method. This gives strong supporting evidence that the active slip system can be identified through rotation caused by localized lattice strain from dislocation pileups. However, it must be noted that it may be necessary to have similar global strain levels

and manifestations of sharp and clear slip bands. This finding enables the use of lattice rotation measurement methods such as EBSD scanning to be used for active slip system identification rather than costly HRDIC scanning.

Furthermore, the direction of the rotation suggested that 11 of the bands had edge dislications of similar sign on either end of the slip band while 6 bands suggested edge dislocations of opposite sign as shown in Figure 6. One possible explanation to the bands that didn't fit either case could be caused by the dislocation pileups being created by screw dislocations form the frank-read loop. This would potentially cause unexpected lattice rotation and may be an area for further study. This shows supporting evidence that the slip bands observed in the material fit the Frank-Read source dislocation formation model.

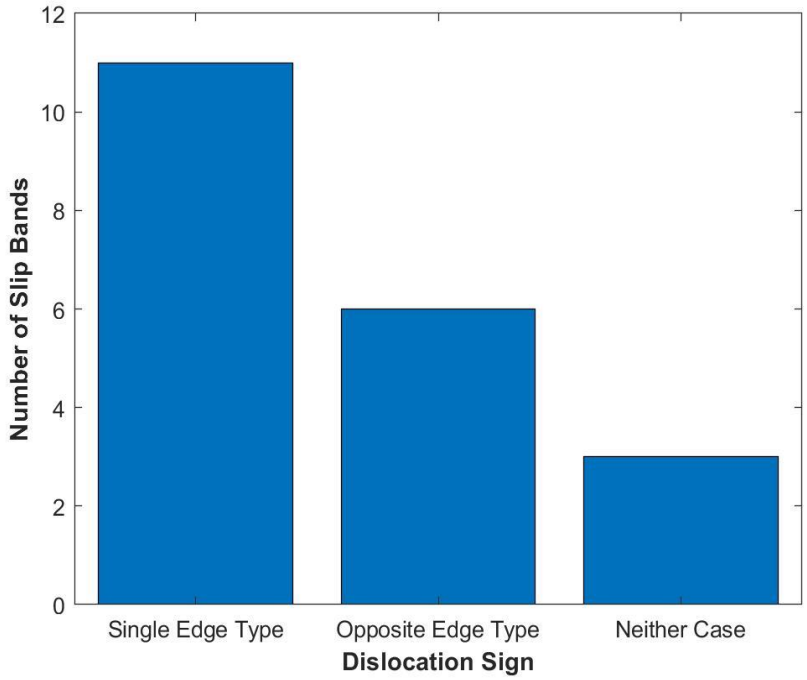

Figure 6. Graph of number of slip bands with single edge dislocation type and opposite edge dislocation type at each end of the band as observed through lattice rotation.

We now consider correlations between the pileup stress measured in the region of GBs, and microstructure characteristics. Data for the relationship between pileup stress and GB misorientation is shown in Figure 7. The maximum pileup stress for a given misorientation value appears to increase with misorientation approximately linearly. However, one can also see that the number of data points also increases with misorientation, then declines; with a final spike in data points at 60°. The 60° GBs represent twin GBs, with approximately 1/3 of the GBs being associated with twins. The distribution of non-twin GB types closely follows the trend noted by Mackenzie [22] for GB misorientation distribution in a random texture, with a peak density at around 40°. If the mean stress is plotted against misorientation (red diamonds), there is no apparent trend; the mean stress is constant with misorientation. Hence, the increase in

maximum stress with misorientation appears to simply be a result of sampling more points, which naturally includes points from further along the tails of the stress distribution.

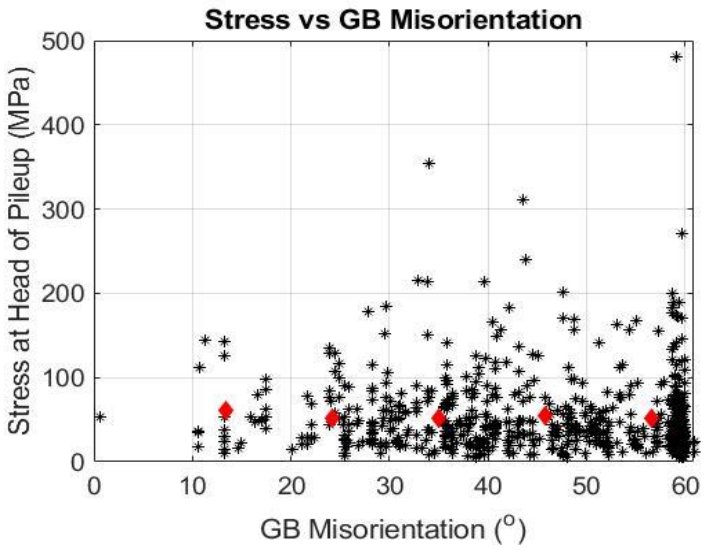

Figure 7. Misorientation vs stress at head of GB pileup. Red diamonds indicate mean stress.

In order to investigate the factors that contributed to the stress distribution at a particular type of GB (in this case, a GB with a given misorientation), the distribution of stress for two different types of GB were considered further. The pileup stress at twin GBs (a total of 212 GBs) and at GBs with misorientation between 35° and 45° (157 GBs) was assessed. Figure 8 shows the data

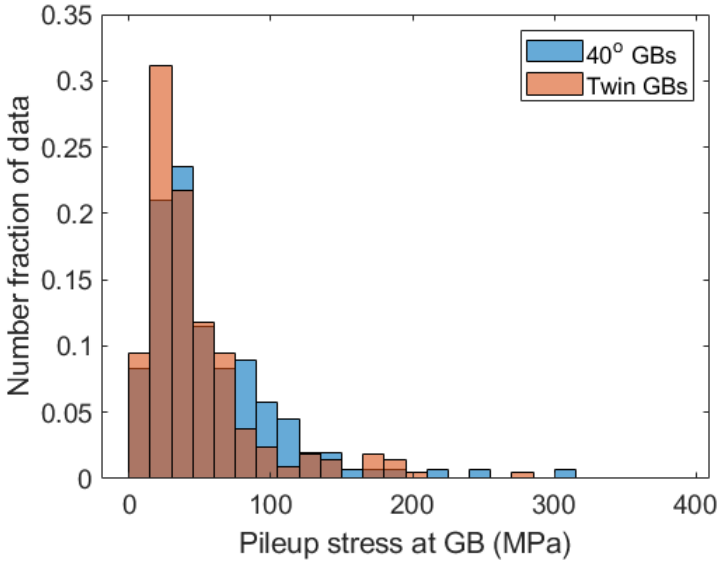

Figure 8. Distribution of pileup stresses observed across 157 GBs with nominal misorientation of 40, and for 212 twin GBs. Note for better visualization of the distribution, the highest twin pileup stress is not shown, but can be seen in fig. 7.

for both types of GB, indicating a log normal distribution of pileup stress; this strengthens the hypothesis that the presence of higher pileup stress at some twin GBs is most likely simply the result of a higher number of data points being sampled from the distribution.

For the pileup stress relating to a single (~40^o) misorientation, various microstructural characteristics were tested for correlation with the level of pileup stress. The strongest correlation related the pileup stress to the maximum shear strain across the relevant shear band. The p-value for the statistical relationship between pileup stress and maximum shear strain along the shear band was almost zero (1e-10), indicating a statistically significant correlation between these factors; on the other hand, the R^2 value for the correlation was only 0.22 (Figure 9), signifying the likelihood that other factors are important. As pointed out by previous researchers, we note that there was no significant correlation between the Schmid factor of the shear bands that develop within a given grain, and the maximum shear that develops.

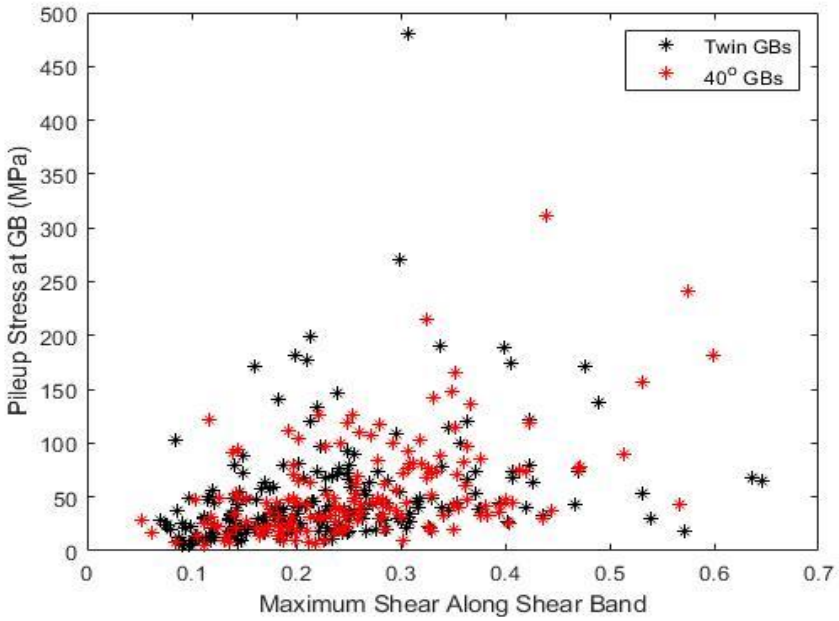

Figure 9. Pileup stress vs maximum shear stress in the band for 157 slip bands with nominally 40 ^{o} misorientation, and for 212 twin GBs in the material.

Importantly, there were no significant correlations between transmissivity factors (the assumed indicators of differing obstacle stress) and pileup stress for a given GB misorientation. Hence the differing pileup stress for a given GB type does not appear to correlate with GB obstacle stress.

In summary, for the case of potential correlations between GB misorientation and pileup stress at the tip of shear bands, the apparent increase in maximum stress with misorientation appears to be due to the higher number of points sampled; the variation in stress for a given GB

misorientation correlates with maximum strain accumulation within the grain, with a relatively weak correlation coefficient that indicates that other factors are also likely to contribute.

We now look for potential correlations between pileup stress and transmissivity factors across all slip bands in the material, without holding the misorientation constant. The m'-factor metric is the simpler of the transmissivity metrics and is similar to the N-factor in terms of definition; the m' and N-factor metrics have a positive linear correlation with R-squared factor of 0.77. Figure 10 illustrates the relationship between transmissivity (as measured by m') and GB misorientation. When the misorientation is low the transmissivity is high (i.e. slip systems in neighboring grains are reasonably well aligned); when the misorientation is high the transmissivity generally decreases but can still take relatively high values at high misorientation values for specific relative orientations. The twin GBs appear to take one of three discrete transmissivity values, with approximately 1/3 of the twins taking each of these values.

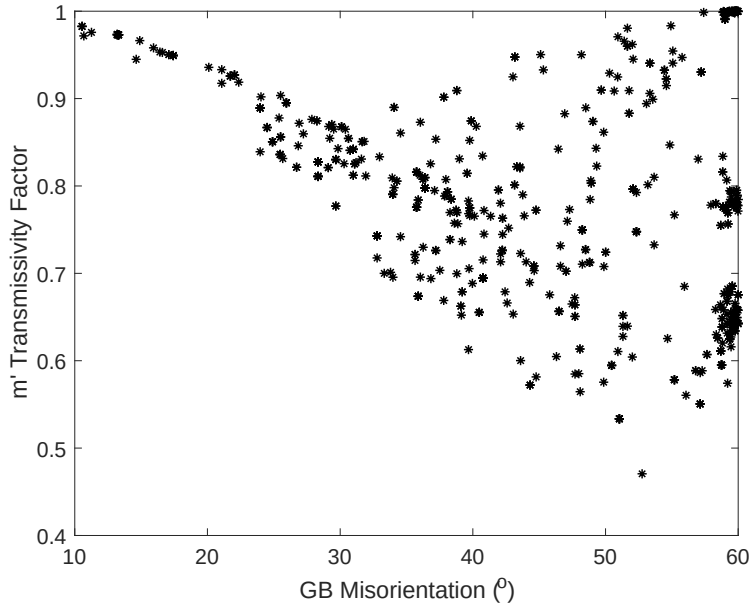

Figure 10. M' transmissivity factor vs misorientation for 660 slip bands.

The relationship between m' factor and pileup stress is shown in Figure 11, **Error! Reference source not found.**and demonstrates a similar trend to GB misorientation – i.e. there is no significant correlation between m' factor and pileup stress. The local average stress with increasing m' factor is almost constant, as shown by the red diamonds in the figure; the higher stress values that appear in the figure correlate with a higher density of points with a specific m' value and are simply drawn from points further along the tails of the log-normal stress distribution as discussed previously.

All other transmissivity metrics considered here (N-factor, λ , residual Burgers vector) display the same independence from the pileup stress. Neither do the Schmid factors of the grain or its neighbor affect the pileup stress distribution. There is also no significant correlation between the angle of the GB trace and the pileup stress. However, there is a weak negative correlation between grain size and maximum stress at the head of the pileup (P value > .005, R-squared value of 0.0288).

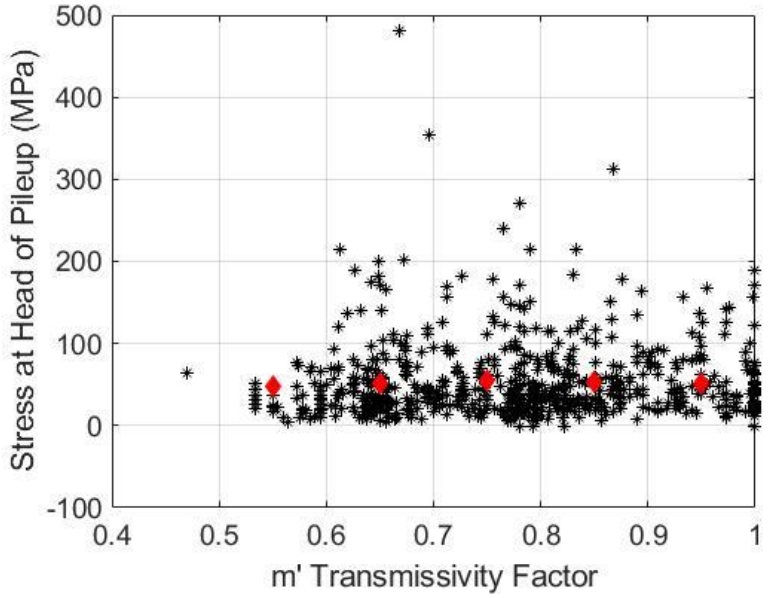

Figure 11. Pileup stress vs m' transmissivity factor for 660 slip bands in the RR1000 material (black asterisks); the mean value for a given m' range is shown as red diamonds.

The previous results, indicating weak or zero correlations between pileup stress and GB character are for the unloaded material; dislocations will certainly reorganize themselves to some extent during unloading. However, the observation of band transmission through a GB will still be apparent after unloading the sample. It was found that 90% of the scanned sample surface demonstrated shear values of less than 0.06 at which point the top ten percent of shear values increased steeply to the maximum shear value in the scans. Therefore, 0.06 was taken to be assumed as no strain. Then through visually inspecting over 35 slip bands and their corresponding shear profiles, it was identified that transmitting slip bands demonstrated unique shear profile behavior at the GB compared to non-transmitting bands. Transmitting bands primarily had shear values above 0.06 at the GB while non-transmitting bands mostly showed the opposite. However, there was some overlap between shear values of about 0.06 and 0.07; therefore, bands with a shear value over 0.07 at the grain boundary were considered to be transmitting to ensure that all bands classified as transmitting do indeed demonstrate transmission. After applying this qualification to all 660 slip bands, it was found that roughly 35% of bands transmit through a grain boundary.

After categorizing transmission events and revisiting the GB pileup stress, it was found that the average pileup stress for transmission events at 66 MPa was almost 50% higher than the average pileup stress of non-transmission events, which was 45 MPa. This could potentially be due to an increase in average stress required to transmit; however, there seems to be no indication of a consistent transmission threshold stress.

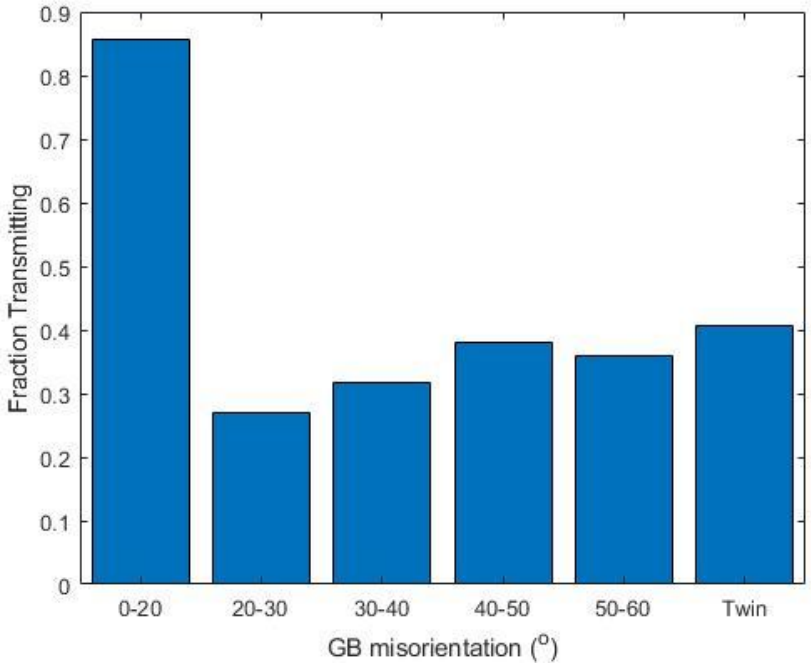

Figure 12. Fraction of transmitting slip bands divided by GB misorientation bins. Low misorientation relates to a high level of transmision.

GB misorientation has a notable influence on slip band transmission. The relationship between transmitting events and GB misorientation is represented in Figure 12. Almost all bands with a low GB misorientation of below 20 degrees transmitted. This fraction of transmitting bands drops off steeply for the 20 to 30 degree GB misorientation set of bands and slowly increases as the GB misorientation increases toward that of a twin boundary where about 40% of the bands show transmission.

Transmission events are also noticeabley influenced by m’ at low misorientation angles and twin boundaries. Figure 14 shows the relationship between the average m’ value in discretized GB misorientation bins for transmitting and non-transmitting events. For misorientations lower than 20 degrees, m’ is clearly a contributing factor of transmission. While there seems to be no distinguishable difference between the transmission and nontransmission events from 20 to 50 degrees, the m’ factor does influence transmission in higher misorientation levels of above 50 degrees.

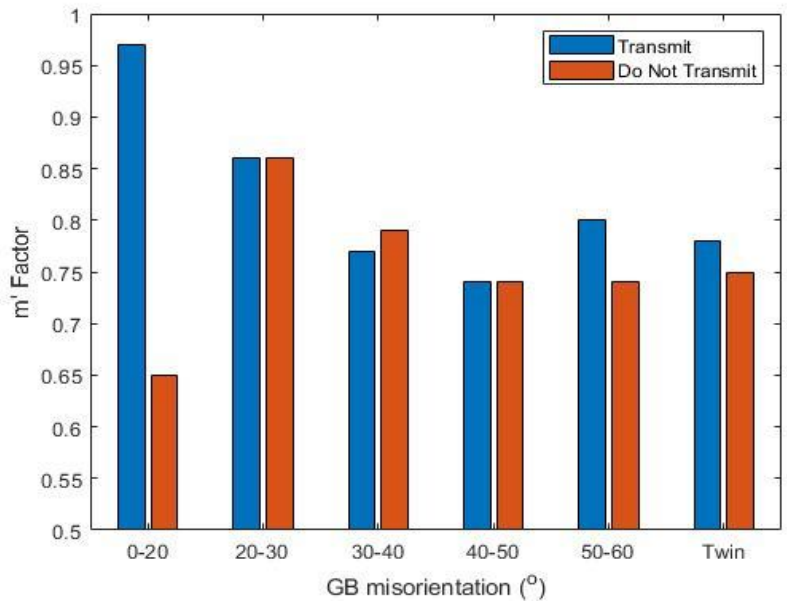

Figure 14. Average m' factor for bands that transmit and do not transmit divided into GB misorientation bins. Low angle misorientations show a significant m' factor difference. Higher misorientations show a real but lower difference in m' factor.

The distribution of m’ factors for transmission events at twin grain boundaries was then investigated. As was mentioned earlier, m’ factor values at twin grain boundaries assumed one of roughly three values which were .65, .78, and 1. Respectively there were 104, 58, and 50 bands that had each of the three values. Figure 13 demonstrates the fraction of transmission

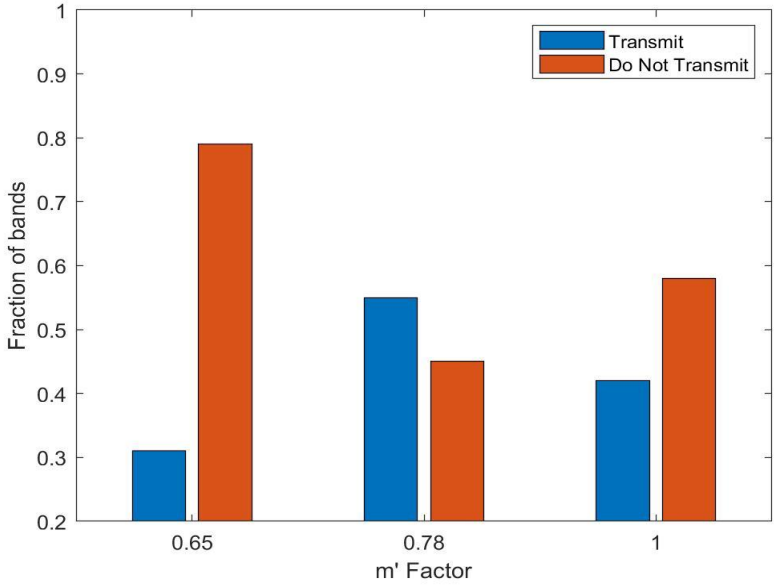

Figure 13. Fraction of bands that transmit at twin GB's divided into the three distinct m' factors found at twin GB's.

and non transmission events for each of these three m' factor values. As can be seen, the peak for transmission events lies at m' factors of roughly 0.78. Overall trends show that transmission increases with m'. However, these data suggest that at twin boundaries, GBs with an m' factor of 1 have a surprisingly lower fraction transmitted than those with m' of 0.78.

In situations where there was complete transmission and two discrete bands were identified on either side of the grain boundary, the maximum shear strain profile provides insightful evidence of dislocation generation. These shear strain profiles were observed from one end of the original slip band, along the band, across the grain boundary to the transmitted band and then on to the opposite end of the transmitted band. It was found that of these events, there were three cases of shear profiles that were observed in decreasing order as follows:

1. A profile containing one maximum found in one grain.
2. A profile containing two local maxima with one found in each grain.
3. A profile containing one maximum at the grain boundary

Figure 15 gives an illustration of the three types of profiles with an example profile of case two. As the maxima of these shear profiles correlate with locations of dislocation generation, this finding provides evidence as to where along the slip band the major dislocation sources lie. Case one suggests that there are instances in which the dislocations are generated in one grain and are transmitted through the grain boundary to the other grain. Case two suggests that there are instances in which dislocation generation is happening in both grains. While case three suggests that there are instances in which the dislocations are primarily generated at the grain boundary. Each one of these dislocation generation points would then correspond with primary Frank-Read dislocation sources for the slip band.

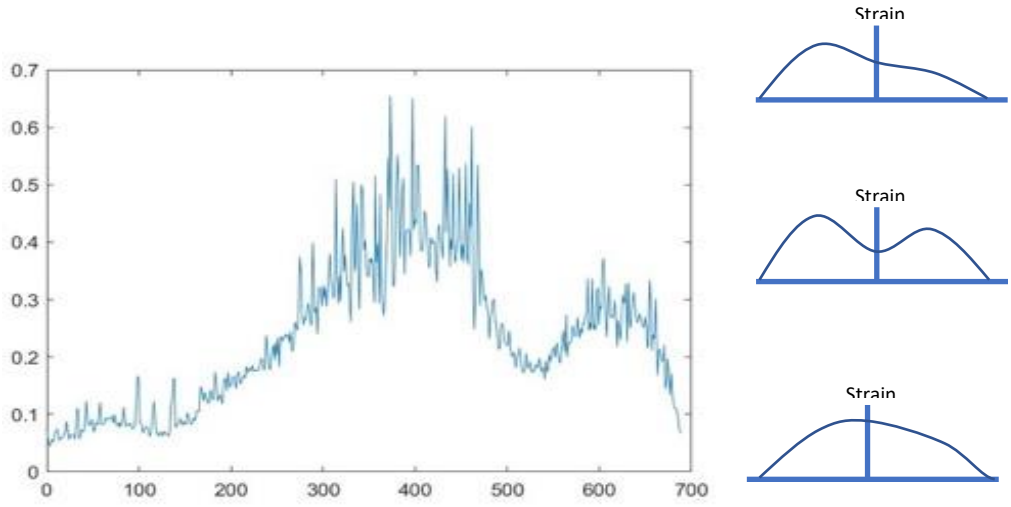

Figure 15. Shear profile of a slip band transmitted through a grain boundary with the local minimum correlating with the GB (left). Diagrams of primary dislocation generation in one grain (top right), both grains (middle right), and at the GB (bottom right).

Conclusion

A gold remodelling process enabled high-resolution strain data to be captured (~117 nm per pixel) of the nickel-based super alloy. This allowed for the shear strain profiles along slip bands to be evaluated. It was noted that the shear strain profile along an 'average' band involved an increase in strain with distance from GB for approximately 1/3 of the grain cross section, followed by a fairly flat region of relatively constant strain, with the strain dropping once again towards the opposite GB for the final 1/3.

The location of peak strain in the central 1/3 of the cross section indicates that nucleation of most dislocations occurs towards the center of grains. We note that in a different tensile test on Inconel 718 by the Manchester group, optical video indicates that slip bands primarily visually nucleated distinctly away from the GB, and then quickly spanned the grain. Other nucleation sources such as nucleation from a separate band transmitting across twin boundaries, nucleation at twin and non-twin grain boundaries were of notable significance, but were not nearly as common as nucleation inside the grain (results are currently being analyzed and compiled for publication).

Based upon the observed strain gradients near GBs, GND spacing follows a similar profile to a single-ended pileup under applied stress, as analyzed by Eshelby and others.

The orientation gradient along a slip band dislocation pileup shows rotation about the line direction as identified by the RDR method. This is a new potential method to identify the active slip system using EBSD scanning alone that can be utilized in tandem with existing slip system identification methods. The direction of the rotation can be indicative of the dislocation sign observed at the surface. This follows characteristics of Frank-Read dislocation sources generating concetric dislocation loops that propagate outwards to either leave the sample surface or become pinned in a dislocation pileup.

The distribution of pileup stresses at GBs, calculated by integrating elastic stresses between GNDs, follows a log-normal distribution that appears to be independent of GB character; i.e. the same stress distribution is present for GBs of all values of misorientation (greater than the minimum defined value of 10 degrees, and including twin GBs), and for all values of the transmissivity factors studied. It appears that all GBs with misorientation above 10 degrees have adequate obstacle strength to resist the pileup stress that the slip bands generate; i.e. the stress associated with the GNDs that form to ensure compatibility is lower than the obstacle strength of all GBs with misorientation greater than 10 degrees.

The pileup stress at the end of a slip band does correlate weakly with the maximum shear stress within a given grain; however, this maximum shear strain does not correlate with the Schmid factor of the grain (an observation that has been made by others).

Transmission is influenced by misorientation and m' values with transmission happening the most at low levels of misorientation. At twin GBs transmission is also influenced by m' which

shows maximum transmission when m’ equals about 0.78. Transmission shear profiles show evidence of dislocation generation in both grains, the grain boundary, as well as generation in one grain with transmission to the other.

Acknowledgements

The BYU and OSU teams work was supported by U.S. Department of Energy (DOE), Office of Science, Basic Energy Sciences (BES), under Awards DE-SC0012587 and DE-SC00012483. Fullwood also gratefully acknowledges the hospitality of the University of Manchester during the development of this work. Allan Harte would like to acknowledge EPSRC Grant EP/T012250/1 for time and resources.

References

[1] E.O. Hall, The deformation and ageing of mild steel: III Discussion of results, Proc. Phys. Soc. Sect. B. 64 (1951) 747–753. doi:10.1088/0370-1301/64/9/303.

[2] N.J. Petch, The Cleavage Strength of Polycrystals, J. Iron Steel Inst. 173 (1953) 25–28.

[3] J.C.M. Li, Y.T. Chou, The role of dislocations in the flow stress grain size relationships, Metall. Mater. Trans. 1 (1970) 1145–1159. doi:10.1007/BF02900225.

[4] Z. Shen, R.H. Wagoner, W.A. T Clark, DISLOCATION PILE-UP AND GRAIN BOUNDARY INTERACTIONS IN 304 STAINLESS STEEL, 1986.

[5] M.D. Sangid, T. Ezaz, H. Sehitoglu, I.M. Robertson, Energy of slip transmission and nucleation at grain boundaries, Acta Mater. 59 (2011) 283–296. doi:10.1016/j.actamat.2010.09.032.

[6] Y. Guo, T.B. Britton, A.J. Wilkinson, Slip band-grain boundary interactions in commercial-purity titanium, Acta Mater. 76 (2014) 1–12. doi:10.1016/j.actamat.2014.05.015.

[7] J.Q. d. F. A. Harte, M. Atkinson, M. Preuss, On the measurement of deformation by electron backscatter diffraction and its suitability as an indicator of local plastic strain, (In Review)., 2019.

[8] F. Di Gioacchino, J. Quinta da Fonseca, Plastic Strain Mapping with Sub-micron Resolution Using Digital Image Correlation, Exp. Mech. 53 (2013) 743–754. doi:10.1007/s11340-012-9685-2.

[9] LaVision, Digital Image Correlation (DIC), DaVis 10. (n.d.). https://www.lavision.de/en/techniques/dic-dvc/index.php (accessed November 6, 2019).

[10] J.M. Gere, B.J. Goodno, Mechanics of materials, Cengage Learning, 2013.

[11] Z. Chen, S.H. Daly, Active Slip System Identification in Polycrystalline Metals by Digital Image Correlation (DIC), Exp. Mech. 57 (2017) 115–127. doi:10.1007/s11340-016-0217-3.

[12] F.C. Frank, W.T. Read, Multiplication processes for slow moving dislocations [7], Phys. Rev. 79 (1950) 722–723. doi:10.1103/PhysRev.79.722.

[13] J.D. Eshelby, F.C. Frank, F.R.N. Nabarro, The equilibrium of linear arrays of dislocations., London, Edinburgh, Dublin Philos. Mag. J. Sci. 42 (1951) 351–364. doi:10.1080/14786445108561060.

[14] M.F. Ashby, The deformation of plastically non-homogeneous materials, Philos. Mag. 21 (1970) 399–424. doi:10.1080/14786437008238426.

[15] D. Hull, D.J. Bacon, Introduction to Dislocations, 2011. doi:10.1016/C2009-0-64358-0.

[16] J.P. Hirth, J. Lothe, Theory of dislocations, Krieger Pub. Co, 1992.

[17] H. Lim, M.G. Lee, J.H. Kim, B.L. Adams, R.H. Wagoner, Simulation of polycrystal

deformation with grain and grain boundary effects, Int. J. Plast. 27 (2011) 1328–1354. doi:10.1016/j.ijplas.2011.03.001.

[18] J. Luster, M.A. Morris, Compatibility of deformation in two-phase Ti-Al alloys: Dependence on microstructure and orientation relationships, Metall. Mater. Trans. A. 26 (1995) 1745–1756. doi:10.1007/BF02670762.

[19] J.D. Livingston, B. Chalmers, Multiple slip in bicrystal deformation, Acta Metall. 5 (1957) 322–327. doi:10.1016/0001-6160(57)90044-5.

[20] E. Werner, W. Prantl, Slip transfer across grain and phase boundaries, Acta Metall. Mater. 38 (1990) 533–537. doi:10.1016/0956-7151(90)90159-E.

[21] M.J. Marcinkowski, W.F. Tseng, Dislocation behavior at tilt boundaries of infinite extent, Metall. Trans. 1 (1970) 3397–3401. doi:10.1007/BF03037870.

[22] J.K. Mackenzie, Second Paper on the Statistics Associated with the Random Disorientation of Cubes, Biometrika. (1958) 229.